Transition Metal Chemistry (2021) 46:263–272
https://doi.org/10.1007/s11243-020-00442-4

Two metal complex derivatives of pyridine thiazole ligand: synthesis, characterization and biological activity

Xunzhong Zou[1] · Pingyi Shi[1] · Ansheng Feng[1] · Meng Mei[2] · Yu Li[1]

Received: 16 October 2020 / Accepted: 8 December 2020 / Published online: 3 January 2021

Abstract

In this work, two new metal(II) complexes with ligand based on pyridine thiazolone group, $[Zn(\mathbf{L})_2(TsO)_2]2DMF$ **(1),** $\{[Cd(\mathbf{L})(NO_3)_2H_2O)]DMF\}_n$ **(2)** (where **L** = 4-(pyridin-4-yl)-2-(2-(pyridin-2- ylmethylene)hydrazinyl)thiazole), were prepared and characterized by physicochemical and spectroscopic methods. In addition, the structure of the complexes (**1** and **2**) was confirmed by single-crystal X-ray analysis. Complex **1** has a discrete monomeric structure where **L** acts as a bidentate agent coordinating the zinc(II) atom through pyridine nitrogen and thiazole nitrogen, while complex **2** consists of polymeric $\{[Cd(\mathbf{L})(NO_3)_2H_2O)]DMF\}_n$ chains in which cadmium(II) atoms are linked by the bridging ligand. The in vitro antimicrobial and antitumor activities of the ligand and complexes (**1 and 2**) were evaluated against seven pathogenic bacterial strains and four human cancer cell lines, and the results showed that some compounds had absolute specificity for certain bacterial strains or cancer cell lines, which thus implied a good application prospect in pharmaceutical use.

Introduction

The successful application of the chemotherapeutic drug cis-diaminedichloroplatinum(II) (cisplatin) in clinical cancer treatment represents the potential biological activity of metal coordination complexes in human diseases [1]. Although heavy metals are trace elements, they play a very important role in all living organisms [2–4]. For example, zinc(II) is related to more than 50 enzymes, and a small amount of cadmium(II) can promote fat metabolism and regulate insulin secretion. Additionally, due to their high bioavailability and strong targeting properties, a large number of coordination complexes that contain zinc(II) and cadmium(II) exhibit good performance in anticancer cell proliferation, as well as in antibacterial and antifungal activities [5–7].

Pyridine thiazole derivatives are known to have interesting bioactive properties, and can be potentially applied in various areas including as inhibitors of the detoxifying enzyme [8], potential anti-diabetes drugs [9], and as potent antibacterial and anticancer agents [10, 11]. Compounds with the hydrazone group and its analogs also have pharmacological potentials due to their unique physiological activity, multidonor ability and bioactivity properties [12, 13]. Therefore, according to the synergistic effect of drug combination principles, the introduction of the hydrazone group into molecules that contain pyridine thiazole is likely to produce stronger biological activity. As was expected, our team was able to report a series of pyridine thiazole derivatives and their complexes, which implied good application prospects for them in pharmaceutical use [14, 15]. In this regard, the synthesis of similar complexes with different coordination sites or metal salts is of interest. Herein, a novel pyridine thiazole derivative of 4-(pyridin-4-yl)-2-(2-(pyridin-2-ylmethylene) hydrazinyl)thiazole was prepared by a cyclization reaction, and complexes $[Zn(\mathbf{L})_2(TsO)_2]2DMF$ **(1),** $\{[Cd(\mathbf{L})(NO_3)_2H_2O)]DMF\}_n$ **(2)** were obtained by coordinating the ligand with $Zn(TsO)_2$ and $Cd(NO_3)_2$,

Electronic supplementary material The online version of this article (https://doi.org/10.1007/s11243-020-00442-4) contains supplementary material, which is available to authorized users.

✉ Meng Mei
meimeng1992@126.com

✉ Yu Li
liyuletter@163.com

[1] Guangdong Research Center for Special Functional Building Materials and Its Green Preparation Technology / Foshan Research Center for Special Functional Building Materials and Its Green Preparation Technology, Guangdong Industry Polytechnic, Guangzhou 510006, People's Republic of China

[2] Wuhan Children's Hospital (Wuhan Maternal and Child Healthcare Hospital), Tongji Medical College, Huazhong University of Science and Technology, Wuhan 430015, People's Republic of China

respectively, and they were then characterized by NMR, elemental analysis (EA), infrared spectroscopy (IR), and single-crystal X-ray diffraction. The inhibitory activities of these compounds against seven pathogenic bacterial strains (*Escherichia coli (E. coli, ATCC* 25922)*, Staphylococcus aureus (S. aureus, CMCC(B)* 26003)*, Salmonella typhimurium (S. typhimurium, CMCC(B)* 50071)*, Bacillus subtilis (B. subtilis, ATCC 6633), Shigella flexneri (Sh. flexneri, CMCC(B)* 51572)*, Vibrio Parahemolyticus (V. Parahemolyticus, ATCC* 17802)*, Pseudomonas aeruginosa (P. aeruginosa, ATCC* 9027)) and four human cancer cell lines (SK-N-SH, HCT-116, AGS and MCF-7) were tested.

Experimental

Materials and physical measurements

Isonicotinaldehyde, 1-(pyridin-2-yl)ethan-1-one, hydrazinecarbothioamide, bromine, zinc(II) p-toluene sulfonate, cadmium(II) nitrate, ciprofloxacin and cisplatin were purchased from Adama Reagent Co. Ltd. All the other reagents and solvents were commercially available and employed as received or purified by standard methods prior to use. SK-N-SH, HCT-116, AGS and MCF-7 were gifts from Doctor Gong Hongjian. Human embryonic lung cell MRC-5 was provided by the Stem Cell Bank at the Chinese Academy of Sciences. Elemental analyses were performed on a Germany Vario EL analyzer (Elementar) and IR spectra on an Avatrar 330 FTIR spectrometer (Thermo Nicolet) with potassium bromide pellets. ^{1}H and ^{13}C-NMR spectra were determined by Bruker AVANCE-III 500 at room temperature in d^6-DMSO, and MestReNova software was used for data analysis and chemical shifts (δ values) are reported as ppm. Biological activity tests were performed on a SpectraMax® ABS Absorbance Reader (Molecular Devices).

Synthesis of 4-(pyridin-4-yl)-2-(2-(pyridin-2-ylmethylene) hydrazinyl)thiazole (L)

The intermediate compounds N-4-Pyridine methylene-thio semicarbazide hydrochloride and 2-bromoacetylpyridine hydrobromide were prepared according to the relevant literature [16, 17]. N-4-Pyridine methylene-thio semicarbazide hydrochloride (10.8 g, 50.0 mmol) and 2-bromoacetylpyridine hydrobromide (14.5 g, 50.0 mmol) were added into 160 mL of 50% ethanol solution at 25℃. After refluxing for 2 h, the mixture was cooled to room temperature and adjusted to neutral pH with 10% sodium hydroxide solution. The resulting solid was recovered through filtration, washed repeatedly with ethanol and dried to give **L** as a yellow powder (Scheme 1). Yield 8.7 g (62%). IR (KBr, cm^{-1}): 3110, 3058, 1578, 1554, 1537, 1474, 1453, 1422, 1369.72, 1293, 1237, 618, 533. ^{1}H NMR (400 MHz, d^6-DMSO, δ ppm): 12.56 (s, 1H, N–H), 7.56–8.64 (m, 8H, pyridine-H), 8.02 (s, 1H, N=CH), 7.36–7.28 (m, 1H, thiazole-H). ^{13}C NMR: (100 MHz, *d*6-DMSO, δ ppm) 168.23 (C from thiazole ring), 155.50, 152.56, 150.62, 149.93, 142.01, 137.72, 123.19, 120.69, 108.90, 97.34. Anal. Calcd. for $C_{14}H_{11}N_5S$ (%): C, 59.77; H, 3.94; N, 24.89; S, 11.40. Found (%): C, 59.70; H, 3.86; N, 24.97; S, 11.43. UV-Vis (DMSO, λmax, nm): 255.0, 355.0. FAB-MS m/z(%): 281.7 ($M^+ + 1$).

Synthesis of the complexes 1 and 2

Metal salt (100 μmol) and **L** (28.0 mg, 100 μmol) were dissolved in methanol (5.0 mL) under reflux conditions for 30 min. The precipitate was recovered by filtration, and then washed with methanol for three times. The resulting dried powder was redissolved with DMF (5.0 mL) and filtered after stirring for 10 min at room temperature. The crystal was obtained in a few days by the method of diethyl ether diffusion (Scheme 2).

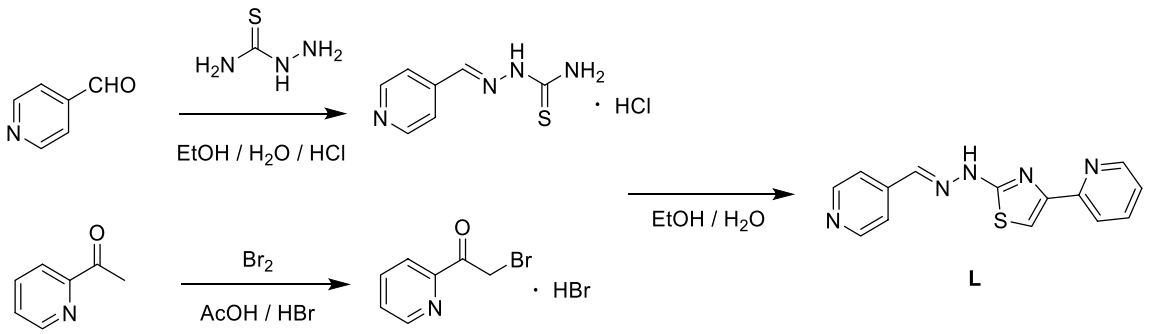

Scheme 1. Synthesis of ligand **L**

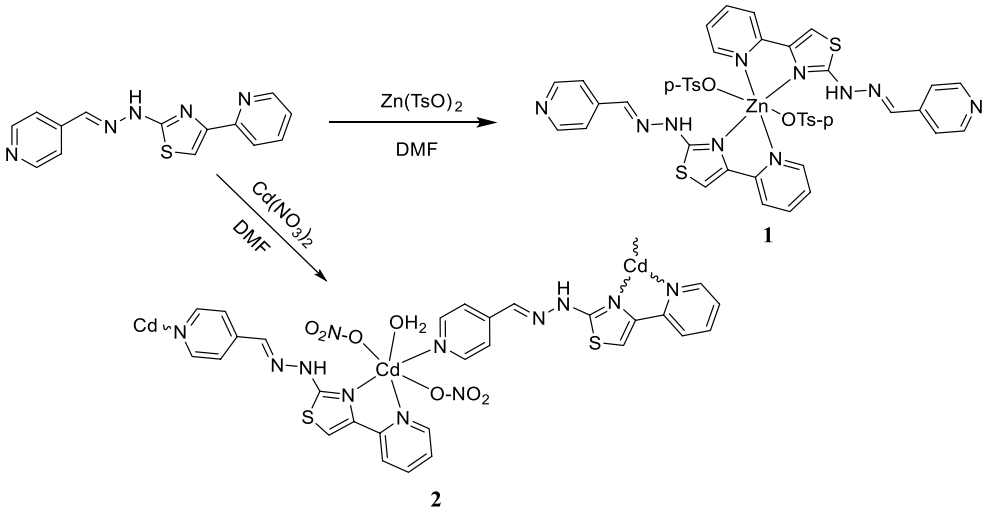

Scheme 2. Synthesis of complexes **1** and **2**

1. Yellow crystals. Yield 30.2 mg (31%). IR (KBr, cm^{-1}): 3096, 3068, 1611, 1579, 1567, 1469, 1445, 1412.94, 1397, 1385, 1348, 1310, 1241. ^{1}H NMR (400 MHz, d^6-DMSO, δ ppm) 12.51 (s, 2H, N–H), 9.02–8.22 (m, 7H), 8.09 (s, 6H), 7.62 (d, 4H), 7.48 (d, 5H), 7.11 (d, 4H), 2.28 (s, 6H, -CH_3). ^{13}C NMR (400 MHz, d^6-DMSO, δ ppm) 165.03 (C from thiazole ring), 155.53, 150.56, 145.90, 138.26, 128.57, 125.96, 120.85, 21.25 (-CH_3). Anal. Calcd. for $C_{48}H_{50}N_{12}O_8S_4Zn$ (%): C, 51.63; H, 4.51; N, 15.05; S, 11.49. Found (%): C, 51.73; H, 4.37; N, 14.90; S, 11.24. MW = 1116.61. UV–Vis (DMSO, λ_{max}, nm): 255.0, 355.0, 490.0.

2. Dark red crystals. Yield 23.3 mg (38%). IR (KBr, cm^{-1}): 3503, 3119, 2980, 2974, 1601, 1566, 1495, 1464, 1413, 1384, 1368, 1288, 1237, 825. ^{1}H NMR (400 MHz, d^6-DMSO, δ ppm) 12.94 (s, 1H, N–H), 8.76 (dd, 2H), 8.70 (dd, 2H), 8.15–8.07 (m, 4H), 7.81 (dd, J = 5.0, 1.5 Hz, 2H). ^{13}C NMR (101 MHz, d^6-DMSO) δ 168.82 (C from thiazole ring), 162.79, 147.86, 147.62, 146.56, 144.89, 138.75, 121.61, 121.53, 113.98. Anal. Calcd. for $C_{17}H_{20}N_8O_8SCd$ (%): C, 33.53; H, 3.31; N, 18.40; S, 5.27. Found (%): C, 33.36; H, 3.41; N, 18.55; S, 5.37. MW = 608.87. UV-Vis (DMSO, λ_{max}, nm): 255.0, 355.0.

X-ray crystallography

The crystallographic data and structure refinement summary of **1** and **2** are listed in Table 1. The crystals of **1** and **2** for X-ray analysis were obtained by ether diffusion. The unit cell and data of the crystals were collected by MoKα radiation (λ = 0.71073 Å) on a SuperNova AtlasS2-CCD diffractometer at 100 K. The collected data were reduced and the multi-scan absorption corrections were performed using CrysAlisPro software [18]. Using Olex2 [19], the structure solution was carried out using SHELXT program [20] and refined by a full-matrix least-squares method based on F^2 against all reflections using SHELXL-2015 [21]. All non-hydrogen atoms were refined anisotropically, while hydrogen atom positions were calculated geometrically and refined using a riding model on their parent C or N atoms. The coordinated *p*-toluene sulfonic acid ion in **1** was found partially disordered over two orientations with a refined occupancy ratio 0.51/0.49. The two orientations are approximately related by a non-crystallographic twofold axis and perpendicular to the benzene ring. The electron density of DMF molecules in **1** has been treated with the program SQUEEZE [22]. DIAMOND [23] was used for molecular graphics.

Antimicrobial activity

Using the microplate reader method, a qualitative analysis for the screening of antibacterial activity was carried out [24, 25]. Mueller–Hinton agar plates were seeded with the indicator bacteria *E. coli, S. aureus, S. typhimurium, B. subtilis, Sh. flexneri, V. Parahemolyticus, P. aeruginosa* and cultured for 24 h at 37 °C. Plates were inoculated with bacteria adjusted to 0.5 McFarland turbidity standards (10^8 cfu/mL). The ligand and complexes (2.0 mg) were added to DMSO (0.2 mL), respectively, and an ultrasound was used to increase their solubility. The resulting solution (10 mg/mL, 2 µL) was added to the enzyme label plate containing 200 µL of liquid culture medium and tested against the 7 pathogenic bacterial strains to determine the inhibitory activity by the absorbance (630 nm) of the bacterial samples using an enzyme-labeled instrument. The antimicrobial activity of the compounds was determined and expressed as the bacteriostatic rate (%). Subsequently, the compounds with a high inhibitory rate (+++) were selected for minimal inhibitory concentration (MIC) determination using the double dilution method with concentrations ranging

Table 1 Crystallographic data and structure refinement summary for **1** and **2**

	1	2
Empirical formula	$C_{48}H_{50}N_{12}O_8S_4Zn$	$C_{17}H_{20}N_8O_8SCd$
Mw	1116.61	608.87
Crystal system	Monoclinic	Monoclinic
space group	I2/a	$P2_1/n$
a/Å	19.0782(17)	7.5203(5)
b/Å	10.0976(8)	14.0164(9)
c/Å	26.484(2)	21.4035(14)
α/°	90	90
β/°	96.693(8)	95.211(6)
γ/°	90	90
V/ Å^3	5067.2(8)	2246.8(3)
Density/g cm^{-3}	1.464	1.800
Z	4	4
μ/mm^{-1}	0.716	1.128
F(000)	2320	1224
Crystal size/mm^3	0.13 × 0.12 × 0.11	0.12 × 0.10 × 0.08
Radiation	(Mo-Kα) 0.71073	(Mo-Kα) 0.71073
Index ranges	−22 ≤ h ≤ 15 −10 ≤ k ≤ 12, −31 ≤ l ≤ 31	−10 ≤ h ≤ 9 −19 ≤ k ≤ 17, −29 ≤ l ≤ 19
θ range for data collection/°	2.150–25.026	2.401–29.597
Goodness-of-fit on F^2	1.038	1.065
Reflections collected	10,884	11,736
Independent reflections	4484 [R_{int} = 0.0450, R_{sigma} = 0.0718]	5295 [R_{int} = 0.0368, R_{sigma} = 0.0621]
Final R indexes [I > = 2σ(I)] R_1, ωR_2	0.0709, 0.1653	0.0377, 0.0611
Final R indexes [all data] R_1, ωR_2	0.1020, 0.1884	0.0515, 0.0678
Data/restraints/parameters	4484/50/369	5295/0/326
Largest diff. peak/hole / e Å^{-3}	0.626/-0.465	0.670/-0.527

from 50 μg/mL to 3.125 μg/mL. The MIC was recorded as the lowest concentration at which the inhibitory rate was greater than 95%. For the blank group, only DMSO was added to the wells, and Ciprofloxacin was used as positive control for antibacterial activity. All tests and analyses were run in triplicate, and the results obtained were averaged. The inhibition percentage was calculated using the following equation:

$$\text{Inhibition}(\%) = \frac{Abs_{\text{blank}} - (Abs_{\text{sample}} - Abs_{\text{control}})}{Abs_{\text{blank}}} \times 100$$

where Abs_{blank} is the absorbance of DMSO + blank medium, Abs_{control} is the absorbance of sample + blank medium, and Abs_{sample} is the absorbance of sample (test samples/standard) + bacterial suspension in medium.

Antitumor activity

The viability of the compounds was tested using the Cell Counting Kit 8 (CCK8) [26–28]. Cisplatin was used as the positive control. Both compounds were dissolved in DMSO and diluted with Phosphate Buffer Saline to the required concentrations (0, 3.125, 6.25, 12.5, 25, 50, and 100 μg/mL). The four human cancer cell lines SK-N-SH, HCT-116, AGS and MCF-7, as well as the normal control cell line human embryonic lung cell MRC-5 were plated in 96-multiwell plates (104 cells/well) for 24 h before treatment with different concentrations of tested samples to allow cell attachment to the wall of the plates, and then cultured using RPMI 1640 or DMEM culture medium containing 10% fetal bovine serum in a 5% (volume fraction) CO2, 37℃ saturated humidity incubator. All cells were treated with compounds for 48 h. The cell growth inhibition rate was determined by using the Microplate Reader to measure the absorbance of each well at 450 nm.

Results and discussion

Synthesis and chemical characterization

The pyridine thiazolone derivative (**L**) was prepared by a cyclization reaction of *N*-pyridine methylene-thio semicarbazide hydrochloride with bromoacetylpyridine hydrobromide in ethanol. **1** and **2** were prepared by the reaction of **L** with $Zn(TsO)_2$ and $Cd(NO_3)_2$ in DMF, respectively, in a molar ratio of 1:1. Crystals of the complexes are soluble in DMSO, DMF and slightly soluble in CH_3OH.

The infrared absorption bands of the main functional groups on **L** and **1**–**2** are listed in Table 2. Additionally, the band at 3415 cm^{-1} in compound **L** might be the stretching vibration band of O–H due to the hygroscopicity of the sample, whereas 2974 cm^{-1} was the stretching vibration band of the C–H bond in the N=C–H group, and the Schiff base ν(C=N) absorption was observed at 1273 cm^{-1}. In complex **1**, the bands at 1445, 1611, and 1567 cm^{-1} were caused by the skeleton vibration of the benzene ring, while a series of strong bands located at 1154–1009 cm^{-1} resulted from the antisymmetric and symmetric stretching vibrations of the SO_3 group in *p*-toluene sulfonate. **2** exhibits typical bands at 1384, 825 cm^{-1}, which were assigned to the characteristic absorption peak of NO_3^- (Fig. S1).

The ^{1}H NMR spectra showed one single peak at 12.56 ppm for **L**, at 12.50 ppm for **1** and 12.94 ppm for **2**, which were all then assigned to the –NH proton of the pyridine hydrazone group (Fig. S2). The signal corresponding to the methyl protons for **1** was observed, which indicated that a coordination reaction had occurred with a model of ML_2. The ^{13}C–NMR peaks at 168.23 ppm for **L**, 165.03 ppm for **1**, 168.82 ppm for **2** were assigned to the thiazole carbon (Fig. S3). The signals of the methyl carbons of *p*-toluene sulfonate for **1** were observed between 20.0 and 40.0 ppm in the ^{13}C–NMR spectra, as expected.

Solution stability of complexes 1 and 2

As a solvent that is used for the preparation of stock solutions for biological activity experiments, DMSO or DMSO-*d*6 was selected to dissolve the complexes and so test the solution stability of the samples by recording the UV-Vis and ^{1}H NMR spectra at different times. The spectra were recorded immediately after dissolution, as well as after 48 h, respectively. As the ^{1}H NMR spectra remained unmodified during this time period, it could be concluded that the corresponding N-pyridine and N-thiazole had remained coordinated to the metal atom and that other coordination reactions did not occur (Fig. S2). Besides, the shape of the spectra and the intensity of the absorption maxima (λ_{max} = 255.0, 335.0, 490 nm for **complex 1;** λ_{max} = 255.0, 355 nm for **complex 2**) were invariable in the UV-Vis spectra (Fig. S4). Furthermore, compared with the spectra of ligand, it was evident that there were no dissociation of metal ions in the DMSO solution, and thus no free metal ions were affecting the biological activity of the complexes. Taken together, the spectroscopic data demonstrated the sufficient stability of complexes **1** and **2** in DMSO solution.

Crystal structures of complex 1

The X-ray crystal structure of **1**, shown in Fig. 1, reveals a neutral complex molecule that consists of a zinc(II) atom and two bidentate **L** ligands. Complex **1** crystallized in a monoclinic unit cell, I2/a space group. The zinc(II) atom was six-coordinated by four nitrogen atoms (Zn1–N1 = 2.138(2) Å, Zn1–N2 = 2.114(3) Å, Zn1–N1^i = 2.138(2) Å, and Zn1–N2^i = 2.114(3) Å) from the ligand and two oxygen atoms (Zn1–O1 = 2.164(2) Å and Zn1–O1^i = 2.164(2) Å) from two toluene sulfonic acid anion, respectively. The presence of a deformed *trans*-N_4O_2 octahedral geometry around the central atom was confirmed by the N1–Zn1–N2 and N1^i–Zn1–N2^i bite angles which were significantly < 90°, whereas the N1–Zn1–N1^i and N1–Zn1–O1^i angles involving the O atom were much greater (99.51(15)° and 97.71(14)°, respectively), and also by the slight difference in bond

Table 2 Infrared absorption bands of the main functional groups on **L** and **1–2**

	L	1	2
Stretching vibration band (N–H)	3110 cm^{-1}	3096 cm^{-1}	3119 cm^{-1}
Skeleton vibration band (Pyridine)	1370, 1578, 1537, 1474 cm^{-1}	1579, 1413, 1397, 1385 cm^{-1}	1566, 1601, 1495, 1464 cm^{-1}
Skeleton vibration band (Thiazole)	1554, 1453, 1422, 1370 cm^{-1}	1469, 1348, 1385 cm^{-1}	1413, 1368 cm^{-1}
Stretching vibration band (C-H on Pyridine)	3058 cm^{-1}	3068 cm^{-1}	2974 cm^{-1}
Stretching vibration band (C=N on ring)	1293, 1237 cm^{-1}	1310, 1241 cm^{-1}	1288, 1237 cm^{-1}
In-plane oscillations band (C–H on Pyridine and thiazole ring)	1100–400 cm^{-1}	1000–400 cm^{-1}	1100–600 cm^{-1}

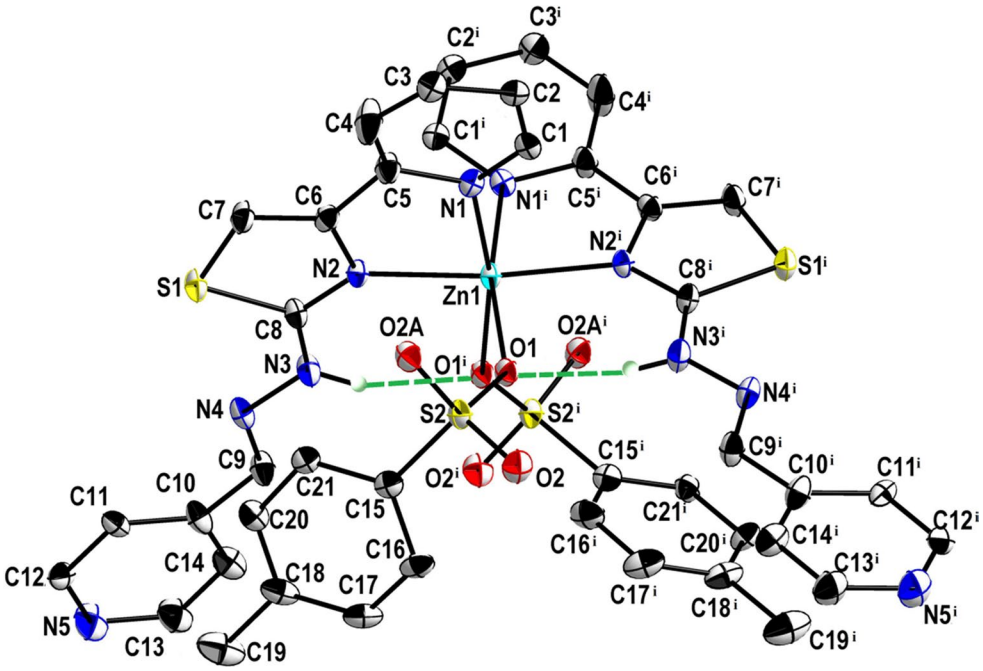

Fig. 1 Molecular structure of **1** with the selected atom numbering scheme. Displacement ellipsoids are drawn at the 30% probability level. H atoms are omitted for clarity. (Green lines indicate the H-bonds)

Table 3 Selected bond lengths (Å) and angles [°] for **1**

Zn1–O1^{i}	2.164(2)	Zn1–N1	2.138(2)
Zn1–O1	2.164(2)	Zn1–N2	2.114(3)
Zn1–N1^{i}	2.138(2)	Zn1–N2^{i}	2.114(3)
O1–Zn1–O1^{i}	89.20(13)	N2–Zn1–O1^{i}	90.14(10)
N1^{i}–Zn1–O1	168.17(9)	N2^{i}–Zn1–O1	90.14(10)
N1–Zn1–O1^{i}	168.17(9)	N2–Zn1–O1	94.48(10)
N1^{i}–Zn1–O1^{i}	90.34(10)	N2^{i}–Zn1–N1^{i}	78.11(10)
N1–Zn1–O1	90.35(10)	N2–Zn1–N1	78.11(10)
N1–Zn1–N1^{i}	92.50(14)	N2–Zn1–N1^{i}	97.35(10)
N2^{i}–Zn1–O1^{i}	94.48(9)	N2^{i}–Zn1–N1	97.35(10)
N2–Zn1–N2^{i}	173.52(14)	N3–H3···O1	2.753(5)

Symmetry transformations used to generate equivalent atoms: (i) 0.5–x, y, 1–z

lengths between the Zn1-O1 and Zn1–N1 bond. Nevertheless, the Zn–O and Zn–N bond lengths are comparable to the corresponding values reported in zinc(II) complexes with pyridine thiazole group that are found in the Cambridge Structure Database [14, 15, 29, 30]. The ligand is slightly twisted with an angle of 1.8(5)° between the thiazole ring plane and the neighbouring pyridine ring plane, and the angles of 12.8(11) between the Schiff base hydrazone plane and the neighbouring pyridine ring plane. The selected bond lengths and angles for complex **1** are summarized in Table 3. Relatively strong hydrogen bonding (N3–H3…O1 = 2.753(5)Å) occurs between the NH group and the coordinated oxygen atoms of the *p*-toluene sulfonic acid anion, and two equivalents of DMF molecules fill interstices between the dimer units.

Crystal structures of complex 2

Complex **2** crystallized in a monoclinic system with a space group of $P2_1/n$ and a six-coordination model of ML. Compared with the discrete 0D monomer structure of **1**, complex **2** represents the basic unit of 1D coordination polymer of $\{[Cd(\mathbf{L})(NO_3)_2H_2O)]DMF\}_n$ (Fig. 2), which is mostly due to the coordinated anionic and solvent molecule(s). With the coordination sphere containing three N atoms from the pyridine thiazole group and three O atoms from two nitrate ions and one water molecule in the structure of **2**, the ligand molecules act as a bridge, forming a one dimensional wavy linear chain with cadmium(II) atoms that works as the connection point (Fig. 2b). The cadmium atom occupies the center of a distorted octahedron geometry which is attributed to the difference of N1^{i}-Cd1-N5, N1^{i}-Cd1-N2^{i}, N1^{i}-Cd1-O3 and N1^{i}-Cd1-O7 bite angles (98.93(8), 72.25(8), 121.15(7), 86.37(8), respectively) as expected, and also attributed to the Cd–N bond (Cd1–N1^{i} = 2.380(2), Cd1–N5 = 2.284(2), Cd1–N2^{i} = 2.302(2)), which is slightly shorter than the Cd–O bonds (Cd1–O3 = 2.3587(19), Cd1–O4 = 2.435(2), Cd1–O7 = 2.334(2)) due to the smaller covalent radius of oxygen. The Cd–O and Cd–N bond lengths are comparable to the corresponding values reported in the cadmium(II) complexes with pyridine ligand [31–33]. The strong hydrogen bonds (N3–H3…O4 = 2.744(5)) meanwhile, were observed between the NH group and one of the oxygen atoms of the nitrate ion. Besides, there was one free DMF molecule in the unit that was not involved in the coordination system. The selected bond lengths [Å] and angles [°] were listed in Table 4.

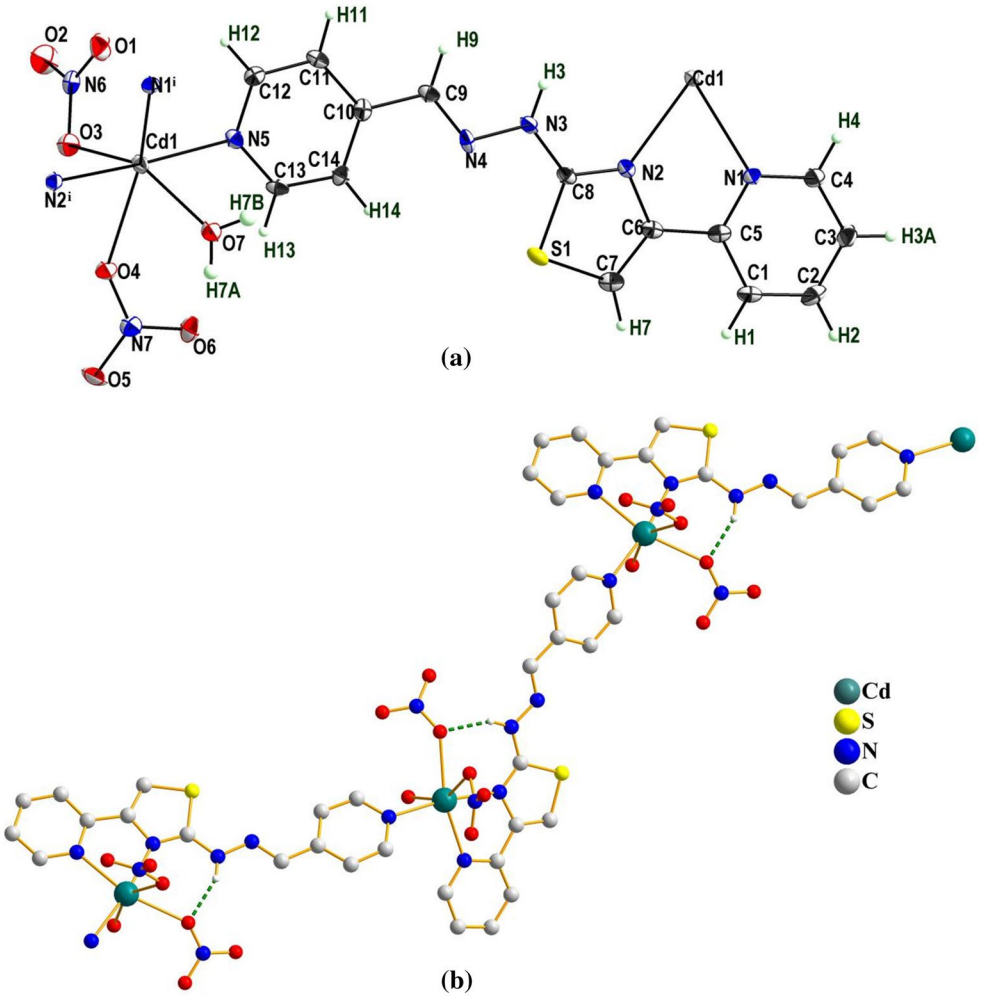

Fig. 2 **a** The molecular structure of **2** with the selected atom numbering scheme. Displacement ellipsoids are drawn at the 50% probability level and solvent molecules are omitted for clarity. **b** One-dimensional chain figure viewed along the *a* axis in **2** (H atoms and solvent molecules are omitted for clarity. Green lines indicate the H-bonds)

Table 4 Selected bond lengths (Å) and angles [°] for **2**

Cd1–O3	2.3587(19)	Cd1–$N1^{i}$	2.380(2)
Cd1–O4	2.435(2)	Cd1–N5	2.284(2)
Cd1–$N2^{i}$	2.302(2)	Cd1–O7	2.334(2)
O3–Cd1–O4	70.96(7)	N5–Cd1–O4	103.41(8)
O3–Cd1–$N1^{i}$	121.15(7)	N5–Cd1–$N2^{i}$	170.41(8)
$N2^{i}$–Cd1–O3	93.53(7)	N5–Cd1–$N1^{i}$	98.93(8)
$N2^{i}$–Cd1–O4	84.35(8)	N5–Cd1–O7	83.84(8)
$N2^{i}$–Cd1–$N1^{i}$	72.25(8)	O7–Cd1–O3	152.25(8)
$N2^{i}$–Cd1–O7	91.71(8)	O7–Cd1–O4	82.49(8)
$N1^{i}$–Cd1–O4	153.73(7)	O7–Cd1–$N1^{i}$	86.37(8)
N5–Cd1–O3	94.35(7)	N3–H3…O4	2.744(5)

Symmetry transformations used to generate equivalent atoms: (i) 0.5 + x, 0.5–y, –0.5 + z; (ii) –0.5 + x, 0.5–y, 0.5 + z

Biological activities

In vitro antibacterial screening of the ligand and its metal complexes (Table 5) was tested against seven pathogenic bacterium at the concentrations of 3.13–50 μg/mL^{-1} in DMSO and compared with the known antibiotic ciprofloxacin. The antibacterial results shown in Table 5 implied that **L** had a good specificity to *B. subtilis* with MICs of 50 μg/mL^{-1} and all the compounds showed low antibacterial activity against *S. typhimurium, V. Parahemolyticus,* and *P. aeruginosa*. Compared with **L**, **1** and **2** had wider broad-spectrum antibacterial properties as well as stronger antibacterial properties against indicator microorganisms at varying degrees. These results suggested that the coordination of metal elements played a key role in the inhibition of the tested microorganisms. As shown in Tables 6, 2 was newly shown to have a significantly improved inhibitory effect on *Sh. Flexneri* with the MIC of 3.13 μg/mL^{-1} and further shown to have higher antibacterial activity than the other compounds against all the tested strains. In addition, when treated with *B. subtilis,* **1** demonstrated even more effective activity than ciprofloxacin with the MIC of 3.13 μg/mL^{-1}. When comparing the antibacterial activities of the ligand and complexes, the enhancement of antibacterial activity in the complexes can be explained on the basis of Overtone's concept and Tweedy's chelation theory [34, 35].

Table 5 Bactericidal activity screening test levels of the compounds (100 μg/mL)

Compounds	*Inhibition ratio/%(Levels* [b]*)*						
	E. coli [a]	*S. aureus* [a]	*S. typhimurium* [a]	*B. subtilis* [a]	*Sh. flexneri* [a]	*V. Parahemolyticus* [a]	*P. aeruginosa* [a]
L	71.3 (++)	76.4 (++)	83.1 (++)	**94.0** (+++)	84.7 (++)	54.8 (+)	70.2 (++)
1	**101.8** (+++)	**95.5** (+++)	60.5 (+)	**95.4** (+++)	89.5 (++)	43.2 (–)	49.7 (–)
2	**100.7** (+++)	**95.3** (+++)	31.6 (–)	**104.4** (+++)	**104.2** (+++)	68.4 (+)	56.6 (–)

Bactericidal activity is revealed by the percentage of complexes against bacterial

[a] *Escherichia coli (E. coli, ATCC* 25922*), Staphylococcus aureus (S. aureus, CMCC(B)* 26003*), Salmonella typhimurium (S. typhimurium, CMCC(B)* 50071*), Bacillus subtilis (B. subtilis, ATCC* 6633*), Shigella flexneri (Sh. flexneri, CMCC(B)* 51572*), Vibrio Parahemolyticus (V. Parahemolyticus, ATCC* 17802*), Pseudomonas aeruginosa (P. aeruginosa, ATCC* 9027*)*

[c] Activity levels: + + ≥ 90%; + + ≥ 70–89%; + ≥ 50–69%; − < 50%

Table 6 MIC (μg/mL) of the compounds against bacterial strains

Compounds	MIC (μg/mL)						
	E. coli	*S.aureus*	*S.typhimurium*	*B.subtilis*	*Sh.flexneri*	*V.Parahemolyticus*	*P.aeruginosa*
CIPRO [a]	12.5	6.25	12.5	6.25	3.13	3.13	6.25
L	–	–	–	50	–	–	–
1	6.25	25	–	6.25	–	–	–
2	6.25	12.5	–	3.13	3.13	–	–

Results are expressed as the minimum inhibitory concentration (MIC)

[a]Ciprofloxacin (CIPRO)

The delocalization of the π-electrons changed the lipophilicity of the complexes which thus favored permeation through the cell membrane.

The in vitro antitumor activity of the compounds against SK-N-SH, HCT-116, AGS, MCF-7 and MRC-5 were measured by CCK8 assay. As shown in Fig. 3a, compounds **L**, **1** and **2** showed a dose-dependent inhibitory effect toward AGS while cisplatin had little effect in its current concentration. Additionally, the complexation of metal ions enhanced the anti-human colon cancer cell HCT-116 activity of **L**, which was reflected by the inhibitory effect of complex **1** in 50 and 100 μg/mL and complex **2** even in 3.125 μg/mL (Fig. 3b). As for MCF-7, complex **1** and the positive control cisplatin showed similar antitumor activity, stronger when compared with **L** but weaker when compared with **2** (Fig. 3c). All tested compounds reduced the cell viability of SK-N-SH. Complexes **1** and **2** showed a better inhibitory effect than cisplatin while **L** did not (Fig. 3d). When the cytotoxic effects of the compounds were examined, the results indicated that all the compounds exhibited low cytotoxicity when the concentration was lower than 25 μg/mL. The toxicity of complex **2** was significantly increased when the concentration of the compound exceeded 25 μg/mL, while the toxicity of other compounds was increased only when reaching 50 or 100 μg/mL (Fig. 3e). Generally, coordination with metal ions enhanced the antitumor and cytotoxicity effect of both complexes **1** and **2**, especially **2**. However, at a concentration of 12.5 μg/mL, complex **2** showed significant antitumor activity with low cytotoxic effects, which thus implied a promising application prospect. Despite the confirmed increasing antitumor activity, a detailed molecular mechanism against the cancer cell lines of the ligand and the complexes remains to be further explored.

Conclusions

We have reported the preparation, characterization and biological activities of a new pyridine thiazolhydrazone derivative and its transition metal(II) complexes named $[Zn(\mathbf{L})_2(TsO)_2]$ **(1),** $[Cd(\mathbf{L})(NO_3)_2H_2O)]DMF$ **(2)**. Single-crystal X-ray diffraction confirmed the geometries of complexes **1** and **2**, showing that **1** featured a mononuclear molecular structure, while **2** was a one-dimensional chain structure. The biological activity of the ligands and complexes were tested against seven bacteria strains and four cancer cell lines. The results showed that complexes coordinated with metal ions had a better antimicrobial and antitumor activity than the corresponding ligand, which might

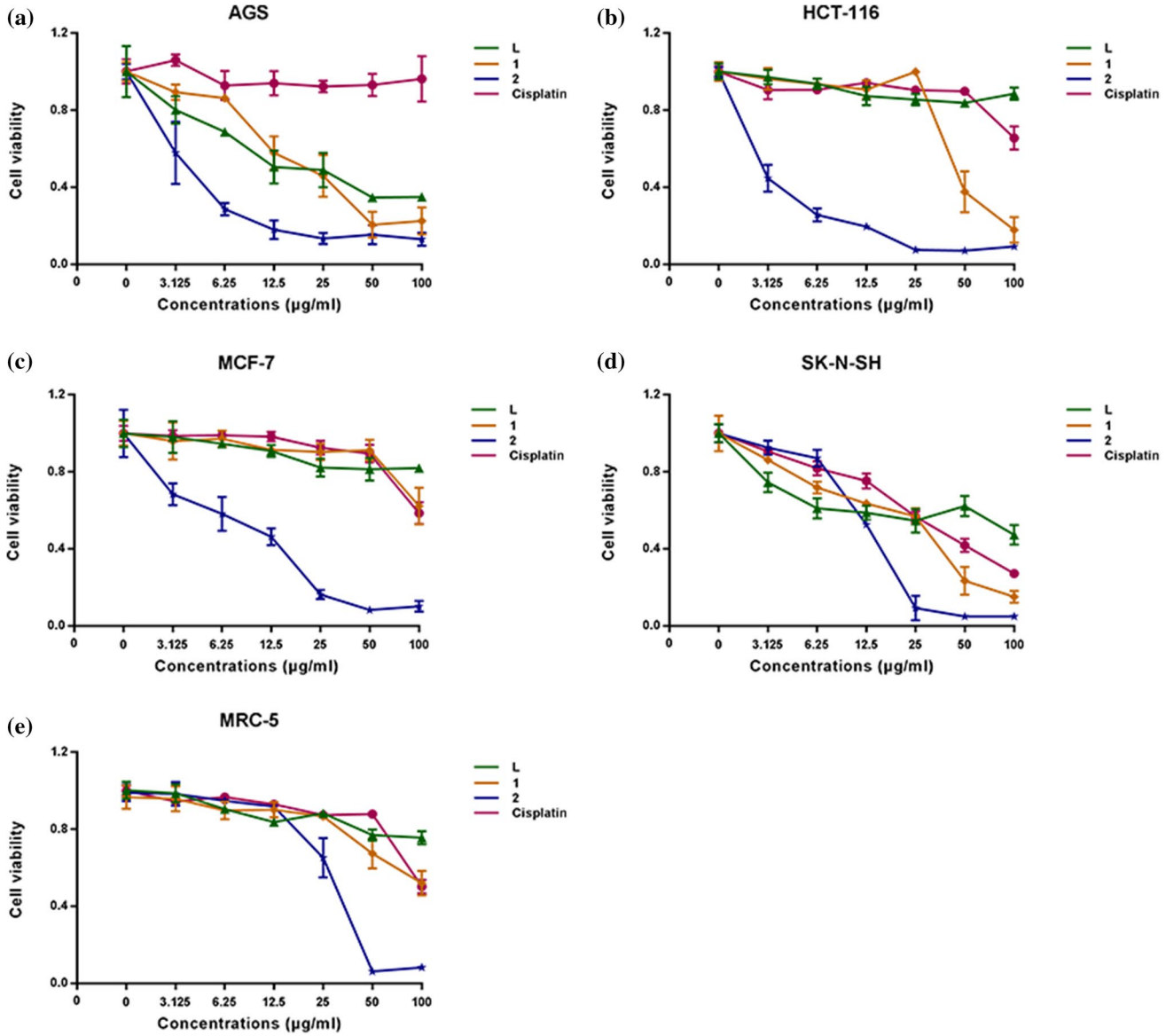

Fig. 3 Dose-dependent antitumor effect of the compounds against human cancer cells. Graphs of cell viability of ligand, the complexes and cisplatin compounds against AGS (**a**) HCT-116 (**b**) MCF-7 (**c**) SK-N-SH (**d**) and MRC-5 (**e**). Data are presented as mean ± SEM for three dependent experiments

provide valuable information for further designing and synthesizing new antimicrobial and antitumor agents.

Appendix A. Supplementary material

Supplementary data associated with this article can be found in the online version, at http://dx.doi.org/ These data include MOL files and InChiKeys of the most important compounds described in this article. CCDC:1,997,854, 1,997,609 contain supplementary crystallographic data for **1** and **2**, respectively. These data can be obtained free of charge via https://www.ccdc.cam.ac.uk/structures/ or the Cambridge Crystallographic Data Centre, 12 Union Road, Cambridge CB2 1EZ, UK; fax: (+44) 1223-336-033; or e-mail:deposit@ccdc.cam.ac.uk.

Acknowledgements The authors thank Gong Hongjian from Wuhan Children's Hospital for providing SK-N-SH, HCT-116, AGS and MCF-7 cell line. This work was financially supported by Guangzhou Science and Technology program (201904010381), Youth innovation Talent project of Guangdong province (2018GkQNCX033), Natural Science Foundation of Guangdong Industry Polytechnic (KJ2019-024).

Compliance with ethical standards

Conflict of interest No potential conflict of interest was reported by the authors.

References

1. Johnstone TC, Suntharalingam K, Lippard SJ (2016) Chem Rev 116(5):3436–3486
2. Munz D, Neumann W (2020) Nachr Chem 1:65–77. https://doi.org/10.1002/nadc.20204093404
3. Bellotti D, Toniolo M (2019) Dudek, Dorota M, Aleksandra G, Matera-Witkiewicz A, Remelli M, Rowinska-Zyrek M. Dalton Trans 48:13740–13752. https://doi.org/10.1039/c9dt02869b
4. Bukonjic AM, Tomovic DL, Stankovic AS, Jevtic VV, Ratkovic ZR, Bogojeski JV, Milovanovic JZ, Djordjevic DB, Arsenijevic AN, Milovanovic MZ (2019) Transit Metal Chem 1:65–76. https://doi.org/10.1007/s11243-018-0270-0
5. Filipovic N, Todorovic T, Markovic R, Marinkovic A, Tufegdzic S, Godevac D, Andelkovic K (2010) Transit Metal Chem 35:765–772. https://doi.org/10.1007/s11243-010-9391-9
6. Popovic A, Nikolic M, Mijajlovic M, Ratkovic Z, Jevtic V, Trifunovic SR, Radic G, Zaric M, Canovic P, Milovanovic M (2019) Transit Metal Chem 44:219–228. https://doi.org/10.1007/s11243-018-0285-6
7. Xu GZ, Li K, Wang L, Zhai YH, Zhang NW (2019) J Coord Chem 72:3057–3070. https://doi.org/10.1080/00958972.2019.1686758
8. Pedras MSC, Abdoli A, Sarma-Mamillapalle VK (2017) Molecules 22(8):1345/1-13451/5
9. Puranik NV, Puntambekar HM, Srivastava P (2016) Med Chem Res 25(4):805–816
10. Chhabra M, Sinha S, Banerjee S, Paira P (2016) Bioorg Med Chem Lett 26(1):213–217
11. Tung TT, Jakobsen TH, Dao TT, Fuglsang AT, Givskov M, Christensen SB, Nielsen J (2017) Eur J Med Chem 126:1011–1020
12. Lapasam A, Banothu V, Addepally U, Kollipara MR (2019) J Mol Struct 1191:314–322
13. Backes GL, Jursic BS, Neumann DM (2015) Bioorg Med Chem 23(13):3397–3407
14. Zou XZ, Feng AS, Liao YZ, Xu XY, Wen HY, Mei M, Li Y (2020) Inorg Chem Comm 118:108030–108034. https://doi.org/10.1007/s11243-019-00314-6
15. Zou XZ, Feng AS, Zeng FR, Lai MC, Liao YZ, Mei M, Li Y (2020). Bioinorg Chem Appl ID. https://doi.org/10.1155/2020/8852470
16. De MC, Carradori S, Secci D, D'Ascenzio M, Guglielmi P, Mollica A, Morrone S, Scarpa S, Agliano AM, Giantulli S (2015) Eur J Med Chem 105:245–262
17. Bhuniya D, Mukkavilli R, Shivahare R, Launay D, Dere RT, Deshpande A, Verma A, Vishwakarma P, Moger M, Pradhan A (2015) Eur J Med Chem 102:582–593. https://doi.org/10.1016/j.ejmech.2015.08.013
18. CrysAlisPro, Version 1.171.37.34 (2014, CrysAlis171. NET), Oxford Diffraction Ltd, Oxford
19. Dolomanov OV, Bourhis LJ, Gildea RJ, Howard JAK, Puschmann H (2009) J Appl Cryst 42:339–341
20. Sheldrick GM (2008) Acta Crystallogr Sect A 71:3–8
21. Sheldrick GM (2015) Acta Crystallogr Sect C 71:3–8
22. Spek AL (2015) Acta Crystallogr Sect C Struct Chem 71(1):9–18
23. Brandenburg K (2009) DIAMOND (version 3.2i) Crystal Impact GbR. Bonn, Alemanha
24. Zhou ZX, Huang QH, Zhu S, Zhou L (2014) WeishengwuQianyan 2:29–35
25. Matsue M, Mori Y, Nagase S, Okamoto S, Sugiyama Y, Hirano R, Kurihara S, Ogai K, Ogura K (2019) Cell trans 12:1528–1541. https://doi.org/10.1177/0963689719881366
26. Li D, Li LF, Zhang ZF, Yan J, Li SZ (2020) J Struct Chem 61(5):789–796. https://doi.org/10.1134/s0022476620050157
27. Li X, Wu Z, Xu L, Chi CL, Chen BQ (2020) Med Chem Res 29(2):180–188. https://doi.org/10.1007/s00044-019-02471-w
28. Li SF, Guo H, Huang Y, Li CM, Liu Y, Han J (2020) J Polym Res 27(3):63–69. https://doi.org/10.1007/s10965-019-2002-3
29. Yang Y, Bian JY, Li YH, Guan HC, Tang YR, Chen YL, Yue SM (2020) J Mol Struct 1202:127219. https://doi.org/10.1016/j.molstruc.2019.127219
30. Zaca TP, Ojwach SO, Akerman MP (2016) Transit Metal Chem 41:663–673. https://doi.org/10.1007/s11243-016-0066-z
31. Zhao R, Li YJ, Chen YF, Cong Y, Zhang J, Dong ZJ, Yuan GM, Cui ZW, Li XK (2019) Polyhedron 166:44–51. https://doi.org/10.1016/j.poly.2019.03.028
32. Zhang JW, Man Y, Ren YN, Liu WH, Liu BQ, Dong YP (2019) Inorg Chim Acta 488:41–48. https://doi.org/10.1016/j.ica.2019.01.004
33. Bullock SJ, Felton CE, Fennessy RV, Harding LP, Andrews M, Pope SJA, Rice CR, Riis-Johannessen T (2009) Dalton Trans 47:10570–10573. https://doi.org/10.1039/b913103e
34. Abele E (2005) Main Group Met Chem 28:45–69
35. Tweedy BG (1964) Phytopathology 55:910–914